Structure and Absolute Configuration of Nyasol and Hinokiresinol via Synthesis and Vibrational Circular Dichroism Spectroscopy

Peter R. Lassen,[†,#] Dorthe Mondrup Skytte,[‡,#] Lars Hemmingsen,[§] Simon Feldbæk Nielsen,[||] Teresa B. Freedman,[⊥] Laurence A. Nafie,[⊥] and S. Brøgger Christensen*[,‡]

The Quantum Protein Centre, Department of Physics, Technical University of Denmark, DK 2800 Lyngby, Denmark, Department of Medicinal Chemistry, The Danish University of Pharmaceutical Sciences, Universitetsparken 2, DK-2100 Copenhagen, Denmark, Department of Natural Sciences, Royal Veterinary and Agricultural University, Thorvaldsensvej 40, DK-1871 Frederiksberg C, Denmark, Lica Pharmaceuticals, Fruebjergvej 3, DK-2100 Copenhagen Ø, Denmark, and Department of Chemistry, Syracuse University, Syracuse, New York 13244

Received August 16, 2005

The absolute configuration of the norlignan (+)-nyasol was determined to be *S* by comparison of the experimental vibrational circular dichroism data with first-principle calculations taking into account the eight lowest energy conformations. The established absolute configuration of (+)-nyasol enables establishment of the absolute configuration of (−)-hinokiresinol, which is concluded to be *S*. A total synthesis and resolution of hinokiresinol has been performed to resolve the conflicting reports of the coupling constant of the vinylic protons of the disubstituted double bond in this molecule. Racemic hinokiresinol was resolved. Both enantiomers possess the same antiplasmodial activity.

Nyasol (**1**) and the *E*-isomer hinokiresinol (**2**) (Chart 1) possessing the skeleton $C_6C_5C_6$ are typical examples of naturally occurring norlignans. The confusion concerning the nomenclature of these two compounds should have been settled by Minami et al.[1] and Oketch-Rabah et al.,[2] who agreed that the *Z*-isomer should be named nyasol and the *E*-isomer hinokiresinol. Unfortunately, confusion concerning the magnitude of the coupling constant of the vinylic protons of the disubstituted double bond in **2** has still not been settled.[3−5]

The first report on the isolation of hinokiresinol from *Chamaecyparis obtusa* did not specify the optical rotation,[6] but a later report established that this plant forms (−)-(**2**).[1] Similarly, no rotation was reported for hinokiresinol isolated from *Libocedrus yateensis*[7] or from *Agathis australis*.[8] Both antipodes of nyasol are naturally occurring. (+)-Nyasol has been isolated from *Asparagus africanus*[2] and *A. cochinchinensis*,[9] and (−)-nyasol has been obtained from *Anemarrhena asphodeloides*.[10,11] A chiral analysis revealed that the nyasol with a specific rotation of $[\alpha]_D$ −67° consisted of 77% of the levorotatory enantiomer and 23% of the dextrorotatory enantiomer, corresponding to a specific rotation of −124° for enantiomeric pure (−)-nyasol.[1]

The absolute configuration of hinokiresinol (**2**) isolated from *Agathis australis* has been assigned as *S* on the basis of correlation with **3** and **4** (Chart 2).[8] However, no specific rotation for the isolated hinokiresinol (**2**) was reported, which makes the determined absolute configuration less authoritative.[8] The correlation is based on comparison of the ORD curve of the dimethyl ether of **2**, formed by thermal conversion of an orthoformate of the dimethyl ether of agatharesinol (**4**), with the ORD curve of the free phenol **2**.[8] The specific rotation of the phenol **2** isolated from *Chamaecyparis obtusa* is −3,[1] whereas the dimethyl ether

Chart 1

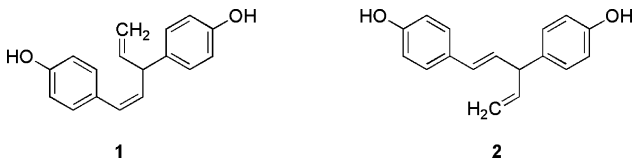

1 **2**

Chart 2

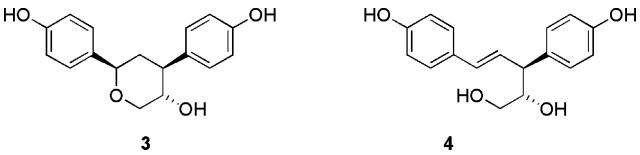

3 **4**

is reported to have a specific rotation of +8.4.[12] Comparison of the ORD curves of these two compounds, thus, should take this shift of sign of the rotation into consideration. The thermal conversion of the orthoformate apparently isomerizes the disubstituted double bond into the *Z*-isomer, since later studies showed that the ^3J coupling of the two vinylic protons at the disubstituted double bond is 12 Hz.[4,5] Such a coupling constant is similar to that reported for nyasol,[2,9] whereas the coupling constant in **2** is 15.9 Hz.[1] This isomerization further questions the conclusion concerning the configuration.

The poor basis for the suggested absolute configuration of hinokiresinol (**2**) and nyasol (**1**) has encouraged us to reinvestigate the absolute configuration of (+)-**2**, isolated from *Asparagus africanus*, by vibrational circular dichroism spectroscopy (VCD). This technique permits comparison of a recorded spectrum with a spectrum calculated from first-principle quantum mechanical methods, i.e., in a nonempirical way.[13] A total synthesis of **2** and comparison of the ^{1}H NMR spectra of **1** and **2** should finally settle the confusion of the magnitude of the coupling constant. Finally advantage was taken of access to the two optical antipodes of **2** to reveal if the antiplasmodial activity was related to the configurational variations. (+)-Nyasol is a modest antiplasmodial agent,[2] but a possible relationship between configuration and antiplasmodial activity has not been investigated.

* To whom correspondence should be addressed. Tel: +45 3530 6253. Fax: +45 3530 6041. E-mail: sbc@dfuni.dk.
† The Quantum Protein Centre.
‡ The Danish University of Pharmaceutical Sciences.
§ Royal Veterinary and Agricultural University.
|| Lica Pharmaceuticals. Present address: Leo Pharma, Industriparken 55, DK-2710 Ballerup, Denmark.
⊥ Syracuse University.
# These two authors have contributed equally to the article.

10.1021/np0502995 CCC: $30.25
Published on Web 10/21/2005

Table 1. Calculated Energies of Gas-Phase Nyasol Conformers (kJ/mol), Relative to the Lowest Energy Structure, as Found Using the MMFF Force Field and Two DFT Methods, B3LYP/6-31G** and B3LYP/AUG-cc-pVDZ[a]

no.	MMFF	B3LYP/6-31G**	B3LYP/AUG-cc-pVDZ
1	0.330200	0.0000	0.0567
2	0.000000	0.0105	0.0000
3	0.402573	0.1444	0.2133
4	0.729980	0.1864	0.1895
5	2.226303	0.2547	1.5526
6	3.039871	0.9321	1.8797
7	2.559570	1.0502	1.9229
8	2.368820	1.2025	2.1405
9	5.528778	4.3426	
10	5.008957	4.4450	
11	6.133102	4.5631	
12	5.669357	4.9753	
13	14.325104	5.4190	
14	14.631180	5.4715	
15	15.171234	5.6002	
16	14.964020	5.6632	
17	19.457092	19.1898	
18	16.850830	19.2134	
19	19.126968	20.7913	
20	19.592728	21.0276	
21	18.936859	21.3007	
22	19.799881	21.5002	
23	19.873138	24.8189	
24	14.858643	24.9974	
25	16.962799	25.3807	
26	17.427505	25.6984	

[a] The conformations are numbered according to the B3LYP/6-31G** energies. The DFT results include thermal free energy contributions calculated using B3LYP/6-31G**.

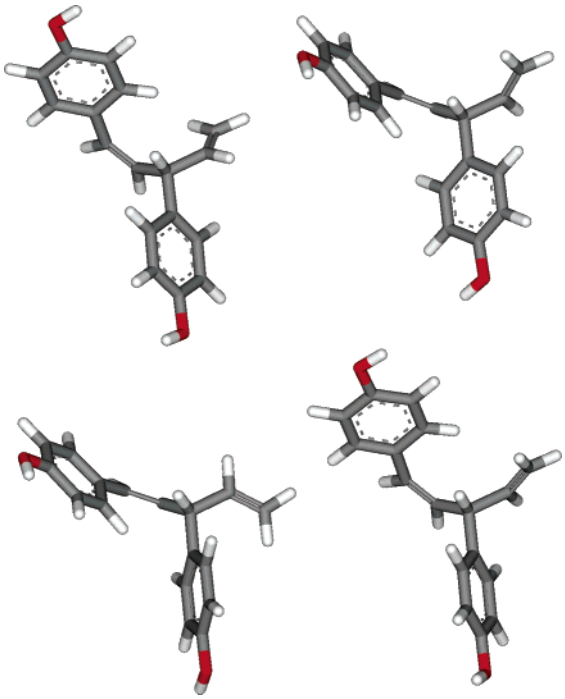

Figure 1. DFT-optimized structures of four (*S*)-nyasol conformers (top left: 1, top right: 5, bottom left: 9, bottom right: 13; numbered according to relative energies, see Table 1), representing the 16 lowest energy conformers. Each structure represents a group of four conformers, which differ only in the relative orientation of the hydroxy groups.

Results and Discussion

Despite the moderate size of **1**, a considerable number of conformers exist at room temperature (Table 1 and Figure 1), with the eight lowest energy structures within 2.1 kJ/mol at the B3LYP/AUG-cc-pVDZ level of theory.

Thus, **1** is among the most flexible small organic molecules studied by VCD spectroscopy. Spectral assignments of theoretical VCD signals are given in Table 2 and Figure 2.

The challenge arises from the fact that the VCD signals from the various conformers tend to extinguish one another, putting high demands on the signal-to-noise ratio of the instrument. There are, however, spectral regions where the first-principle calculations predict that most conformers give similar VCD signals, allowing determination of the absolute configuration of nyasol (Figure 3).

In particular the strong positive signal at 1510 cm^{-1} observed for nyasol dissolved in DMSO-d_6 (Figure 4) and the spectral signatures at 800−1000 and 1590−1650 cm^{-1} observed for nyasol in a KBr pellet (Figure 5) are such regions.

The pronounced similarities between the recorded spectrum of (+)-nyasol and the calculated spectrum for (*S*)-nyasol in these regions therefore show that (+)-nyasol possesses the *S*-configuration. There are discrepancies between experimental and calculated spectra, particularly in the region from 1100 to 1300 cm^{-1}, for both the IR absorption and VCD signals. The most intense signals in this region originate from vibrations involving the two hydroxy groups of nyasol, indicating that the broadening and changes in frequencies and relative intensities of the signals are due to nyasol−solvent and/or nyasol−nyasol interactions. These intermolecular interactions tend to broaden the signal from the C−O stretching vibration at 1270 cm^{-1} and almost extinguish the O−H bending at 1170 cm^{-1}. Their combined vibration at 1620 cm^{-1} is less affected. The quenched O−H bending has been reproduced theoretically by calculating spectra with one explicit DMSO molecule next to each of the two hydroxy groups, putting the qualitative interpretation on more firm theoretical grounds. UV−vis absorption and conventional (electronic) CD spectra were also recorded for nyasol from *A. africanus* (see Figure 6), and given the assignment derived from the VCD experiments, we conclude that the CD spectrum corresponds to (*S*)-nyasol.

Minami et al.[1] have similarly utilized CD data in the assignment of absolute configuration of nyasol and hinokiresinol, in agreement with the data presented in Figure 6. Their findings prove that (−)-nyasol is hydrogenated to the antipode of the tetrahydro derivative of (−)-hinokiresinol. Consequently the parent compounds (−)-nyasol and (−)-hinokiresinol must possess opposite absolute configurations as well. Since (+)-nyasol is *S*-configured, (−)-nyasol must possess the *R*-configuration. (−)-Hinokiresinol has the opposite configuration, that is, *S*, and consequently (+)-hinokiresinol possesses the *R*-configuration as previously concluded.[8]

Synthesis of Hinokiresinol (2). Some synthetic methods for the dimethyl ether of **2** have been published.[6,14] The synthesis of the dimethyl ether of hinokiresinol is initiated by an addition of a Grignard reagent to an oxo compound, preventing the direct synthesis of hinokiresinol with free phenolic groups.

In the only reported synthesis of the free diphenol **2**[15] the phenolic hydroxyl groups were protected as *tert*-butyldimethylsilyl ethers (TBDMS). The TBDMS group was cleaved during the initial Claisen−Schmidt condensation and had to be reintroduced in a modest yield. This problem was overcome by protecting the phenolic groups as tetrahydropyranyl ethers. This protecting group survived the condensation of the ketone and the aldehyde to give **5**, which smoothly reacted with vinylmagnesium bromide to give **6**. Addition of copper(I) iodide ensured 1,4-addition of the Grignard reagent. Sodium borohydride

Table 2. Assignment of Selected Peaks in the B3LYP/AUG-cc-pVDZ-Calculated IR and VCD Spectra for the Lowest Energy Conformer[a]

ν (cm^{-1})	ϵ ($M^{-1}\,cm^{-1}$)	$10^4\Delta\epsilon$ ($M^{-1}\,cm^{-1}$)	assignment
846	43.267	−263.076	phenol C−H oop bend
849	96.499	323.353	phenol C−H oop bend
859	54.035	−49.5495	phenol C−H oop bend
888	79.521	−42.1694	methine C−H bend
949	23.575	26.0106	vinyl C−H oop bend
959	55.749	−4.53252	vinyl C−H oop bend
1005	22.618	−4.70156	vinyl C−H oop bend
1025	36.633	13.4051	vinyl C−H ip bend
1120	33.284	−75.0412	phenol C−H ip bend
1127	33.226	−7.48434	phenol C−H ip bend
1184	482.469	96.6739	O−H bend
1186	161.730	−92.2848	O−H bend
1189	253.009	−23.8879	O−H bend
1269	124.863	78.9772	C−O stretch, methine C−H bend
1273	207.496	−39.1544	C−O stretch, methine C−H bend
1279	197.746	−84.5487	C−O stretch, methine C−H bend
1322	15.465	97.8881	vinyl C−H ip bend
1367	87.202	−40.1792	phenol C−C stretch, C−H and O−H ip bend
1369	73.435	33.0594	Phenol C−C stretch, C−H and O−H ip bend
1423	57.911	−27.8639	vinyl C−H ip bend
1434	35.367	−19.088	vinyl C−H ip bend
1464	37.615	111.113	phenol C−H, O−H ip bend
1535	276.918	22.9206	phenol C−O stretch, C−H ip bend
1539	257.528	146.532	phenol C−O stretch, C−H ip bend
1625	42.569	−55.4286	phenol C−C stretch
1634	48.017	−5.691	phenol C−C stretch
1653	186.086	2.0246	phenol C−C stretch
1654	94.705	−5.97896	phenol C−C stretch
1689	7.045	−25.3217	vinyl C−C stretch
1693	38.819	−76.3316	vinyl C−C stretch

[a] Columns are wavenumbers ν, molar absorptivities ϵ, differential absorptivities $\Delta\epsilon$, and assignments. Abbreviations: ip = in-plane, oop = out-of-plane.

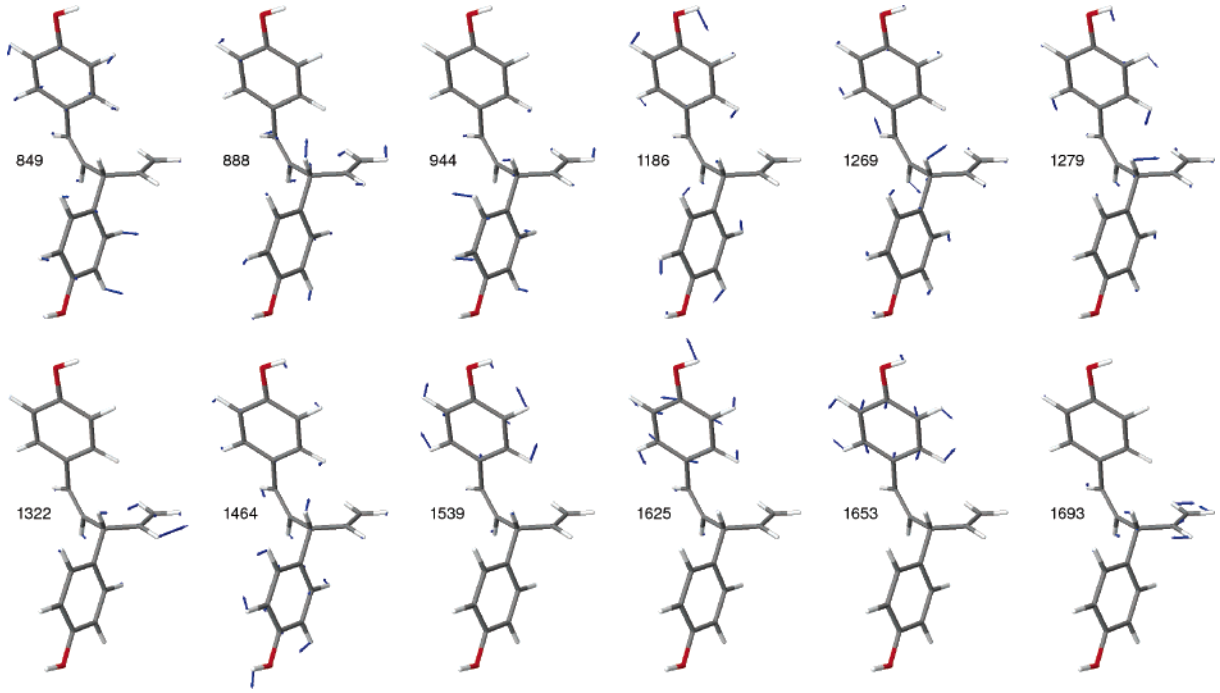

Figure 2. Relative amplitudes of selected vibrational modes assigned in Table 2 for the lowest energy conformer, calculated using B3LYP/AUG-cc-pVDZ. Each mode is labeled with the corresponding wavenumber (cm^{-1}).

reduction of the ketone yielded a mixture of the diastereomeric alcohols **7**. A further advantage of the tetrahydropyranyl group was that a hydrochloric acid-catalyzed elimination of water from **7** simultaneously cleaved the protecting groups. In addition all the steps in the reaction sequence in Scheme 1 afforded better yields than the reaction sequence using the TBDMS protecting group. No nyasol was detected in the reaction mixture. The vinylic coupling constant was found to be 15.9 Hz, as expected for a *trans* coupling.

Optical resolution was performed by chiral HPLC to give the two enantiomers having identical ^{1}H NMR spectra.

The antiplasmodial effect of the two enantiomers of **2** was determined. Surprisingly, the enantiomers were equi-

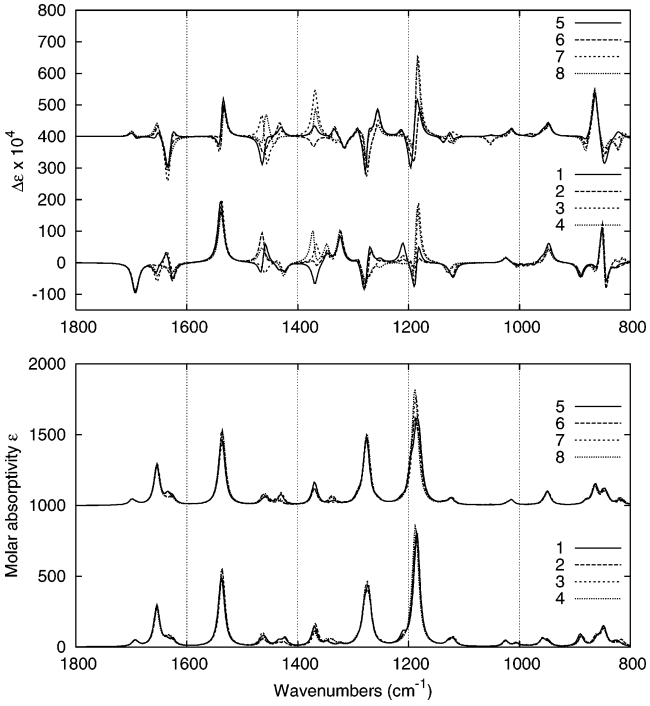

Figure 3. Calculated IR absorption (lower half) and VCD spectra (upper half) for the eight lowest energy conformers of (*S*)-nyasol, at the B3LYP/AUG-cc-pVDZ level of theory. Frequencies are not scaled. The bands are plotted as Lorentzians with half-widths of 6 cm^{-1}. Half of the spectra are offset for clarity.

potent [IC_{50} values: *rac*-**2**, 51 ± 10 μM; (+)-**2**, 55 ± 14 μM; (−)-**2**, 80 ± 25 μM]. The antiplasmodial activity, thus, is not dependent on the absolute configuration.

Experimental Section

General Experimental Procedures. IR and VCD spectra were obtained on a Chiral*IR* FT-VCD spectrometer (BioTools, Inc., Wauconda, IL), equipped with two sources[16] and two photoelastic modulators[17] optimized at 1400 cm^{-1}. An optical band-pass filter was used to allow only the spectral region 800−2000 cm^{-1} to reach the detector. Spectra were calibrated automatically, using the standard calibration files.

VCD spectra were recorded both in DMSO-d_6 solution (5 mg of nyasol in 100 μL of DMSO-d_6 in a BaF_2 cell with 100 μm path length) and in KBr pellets (250 mg KBr, ϕ 13 mm × 1 mm). The resolution was 8 cm^{-1}, and the acquisition time was 9 h for DMSO-d_6 solution and 31 h for the KBr pellet. In the latter case, spectra from two different orientations of the KBr pellet were averaged to reduce the baseline offset. ^1H NMR spectra were recorded on a Varian Mercury spectrometer or Varian Gemini 2000 spectrometer at 300 MHz using tetramethylsilane as internal standard. Splitting patterns are described as singlet (s), doublet (d), triplet (t), doublet of doublets (dd), doublet of double doublets (ddd), and multiplet (m). Uncorrected melting points were determined on a Büchi SMP-20 apparatus, and optical rotation was measured on a Perkin-Elmer 241 polarimeter. Column chromatography was performed on silica gel 60 (Merck 107734). For HPLC a Waters 6000A pump and a Shimadzu SPD 6A detector was used. THF was distilled from LAH and kept over molecular sieves. UV−vis absorption spectra were recorded on a Cary 5 spectrometer, and conventional (electronic) CD spectra were recorded on a JASCO-720 CD instrument using a cylindrical quartz cuvette with a light path of 5 μm and a 61 mg/mL solution of nyasol in MeCN. Using MeOH as solvent does not change the spectra significantly. The instrument was purged with N_2. All spectra were baseline corrected using a baseline recorded with no cell in the instrument and collected at room temperature.

Computational Methods. Conformational searches and geometry optimizations of (*S*)-nyasol were performed with MacroModel (Schrödinger, Portland, OR).[18] Conformational searches were made in the gas phase using systematic torsional search (SUMM) and an energy window of 20 kJ/mol. For each structure the structure was optimized using the MMFF force field, with 500 steps, 1000 iterations, and a threshold of 0.05. The (unique) structures from the conformational search were subsequently geometry optimized using density functional theory (DFT) as implemented in Gaussian 03,[19] using the B3LYP functional[20] with the 6-31G** and AUG-cc-pVDZ basis sets and default convergence criteria.[21,22] Vibrational spectra were calculated with the same methods. Dipole and rotational strengths from Gaussian were converted into molar absorptivities[13] (M^{-1} cm^{-1}), and each spectrum was plotted as a sum of Lorentzian bands with half-widths of 6 cm^{-1} for comparison with experiments. The relative energies presented include free energy corrections from molecular vibrations.

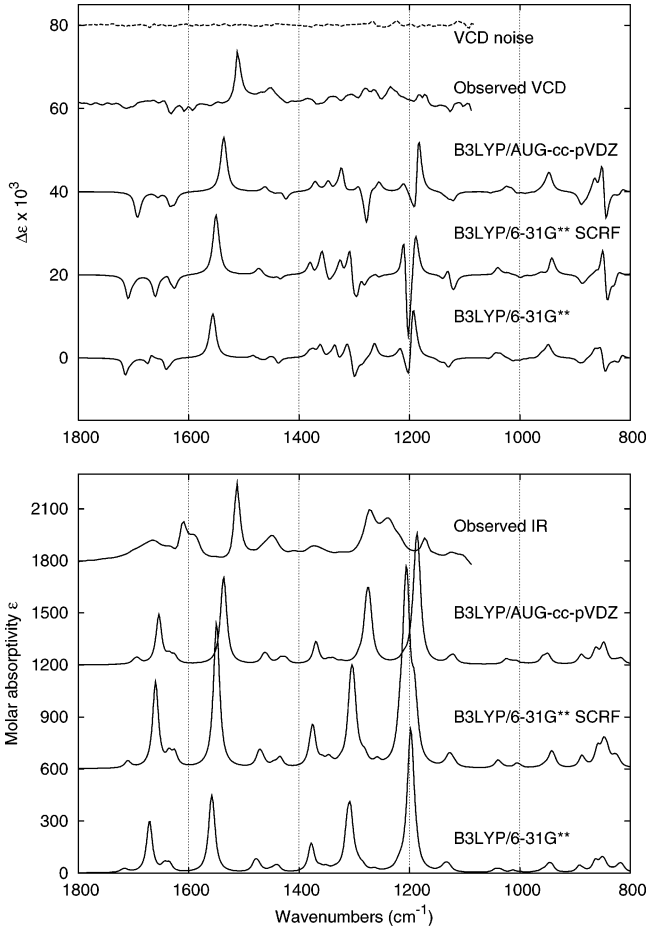

Figure 4. Comparison of observed and calculated IR absorption (lower half) and VCD (upper half) spectra of nyasol. Experimental spectra are measured in DMSO-d_6, using a resolution of 8 cm^{-1} and 9 h acquisition time, with the instrument optimized at 1400 cm^{-1}. VCD noise is shown in the uppermost (dashed) trace. Experimental IR absorption spectra are corrected for the presence of solvent, and spectra are offset for clarity. Calculated spectra are Boltzmann-weighted averages of the eight lowest energy conformers of the *S*-enantiomer, with three different DFT methods as indicated. The B3LYP/6-31G** SCRF uses a continuum solvent model for DMSO.

Nyasol Conformers. In both the gas phase and solvent, the conformational searches of (*S*)-nyasol yielded 26−29 structures within the energy window. A few of these structures converged to the same local minimum at the B3LYP/6-31G** level of theory. All energies from gas-phase geometry optimizations in MacroModel and Gaussian 03 are shown in Table 1, where the conformations are numbered in order of the B3LYP/6-31G** energies. In most cases the MMFF force field performs very well, but there are cases where the relative energy deviates by up to 8 kJ/mol from the first-principle calculations.

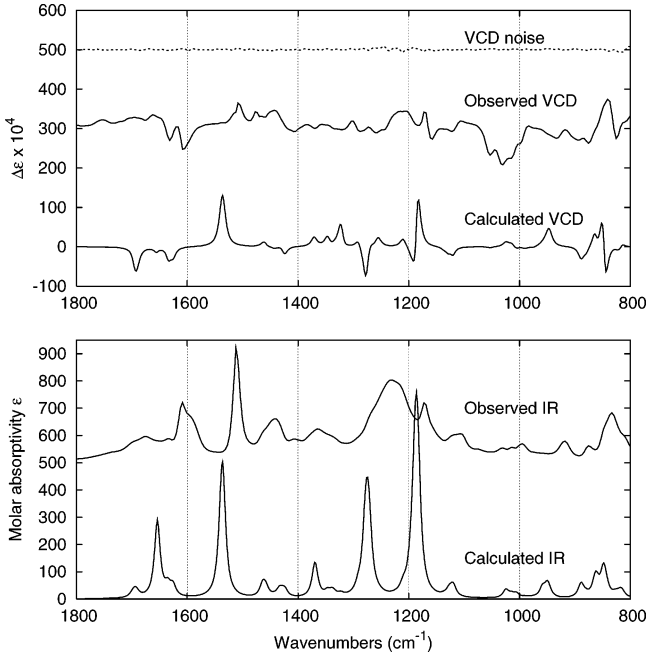

Figure 5. Observed IR absorption (lower half) and VCD (upper half) spectra of nyasol in a KBr pellet, compared to the DFT calculation for (*S*)-nyasol using B3LYP/AUG-cc-pVDZ. The experimental resolution is 8 cm^{-1}, with the instrument optimized at 1400 cm^{-1}. The total acquisition time is 31 h, and spectra from two different orientations of the KBr pellet were averaged to reduce the baseline offset. VCD noise is shown in the uppermost (dashed) trace.

A representative selection of the gas-phase structures are shown in Figure 1, arranged in order of increasing energy. The conformational energy displays gaps of about 3 kJ/mol between conformers 8 and 9 and of about 14 kJ/mol between conformers 16 and 17. In the analysis of the VCD spectra we have therefore included only the eight lowest energy conformers. Furthermore, the conformational energies of the 16 lowest energy conformers fall into groups of four having rather similar energies, because both hydroxy groups can point in two almost equally favorable orientations. Within each group of four conformers, the carbon skeleton is basically fixed, and only the hydroxy group orientations differ. No considerable geometry changes in the gas-phase structures occur when DFT optimization includes a self-consistent reaction field (SCRF) solvent model (polarizable continuum model)[23] for DMSO.

Infrared and VCD Spectra. Figure 3 depicts the calculated IR and VCD spectra for the eight lowest energy structures, calculated using the B3LYP functional and AUG-cc-pVDZ basis set. The spectra of conformers 5−8 are offset for clarity. All of the conformations have very similar IR spectra, differing mostly in frequency and intensity of some minor peaks. However, in the calculated VCD spectra, considerable differences arise between the conformers To determine the absolute configuration, we identified the spectral regions in Figure 3 with the least variability. These regions will be optimal for determinations of the absolute configurations of nyasol, as the signals from different conformers do not extinguish each other to any significant extent. These regions are 800−1000, 1250−1350, and 1510 cm^{-1}, and the negative amplitude signals around 1650−1700 cm^{-1}. To distinguish conformers in the observed spectra, we note that the band around 1530 cm^{-1} has a different shape for the two groups of conformers (1−4 and 5−8). Additionally, around 1300 and 1650 cm^{-1}, there seem to be consistent differences between these two groups.

Assignments for the lowest energy conformer are shown in Table 2.

In Figure 4 the recorded spectrum (DMSO-d_6 solution) of (+)-nyasol isolated from *A. africanus* as previously reported[8] is compared to the Boltzmann weighted average of the calculated spectra for the eight lowest energy conformers,

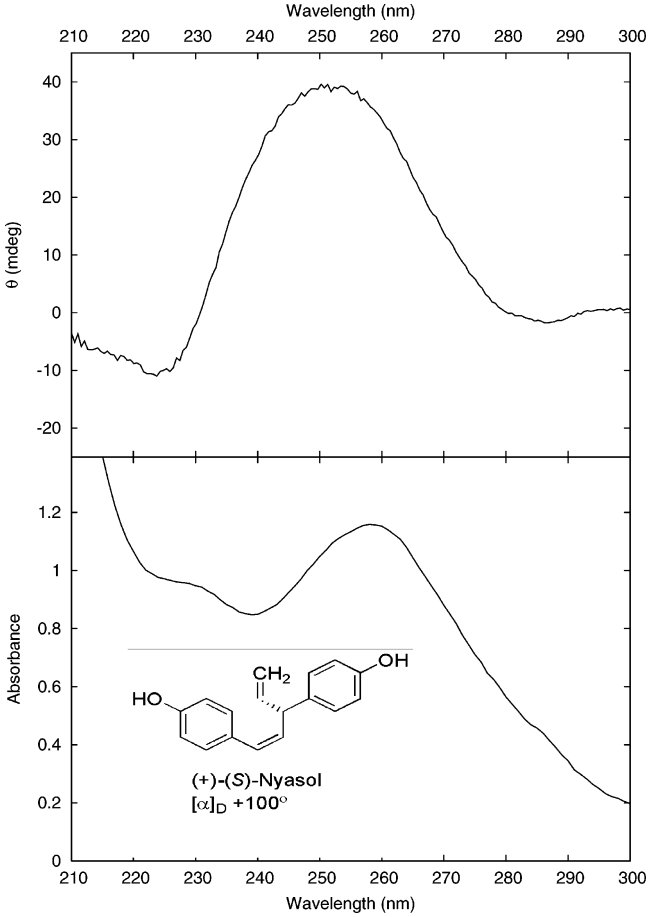

Figure 6. UV−vis absorption (bottom) and CD (top) of (+)-(*S*)-nyasol in MeCN (61 mg/mL), path length of 5 μm. Based on the assignment derived from the VCD spectra, the CD spectrum represents (*S*)-nyasol.

using B3LYP/6-31G**, B3LYP/6-31G** with an SCRF continuum solvent model for DMSO, and B3LYP/AUG-cc-pVDZ, respectively. The solvent DMSO-d_6 obscures the spectrum below 1100 cm^{-1}. In the 1250−1350 cm^{-1} region the VCD signals are too weak to reliably determine the absolute configuration, but above 1400 cm^{-1} the experimental spectrum of (+)-nyasol and the calculated spectrum for *S*-nyasol compare well. Similarly, there are considerable differences between the calculated and observed IR absorption signals in the 1180−1300 cm^{-1} region. In Figure 5 the (+)-nyasol containing a KBr pellet measurement is compared to the B3LYP/AUG-cc-pVDZ calculation for *S*-nyasol, which shows very good agreement in the region 800−1000 cm^{-1} and reasonable agreement above 1300 cm^{-1}. The nyasol concentration differs between the DMSO-d_6 solution and KBr pellet experiments, and consequently different spectral regions have optimal IR absorption for VCD measurements. Thus the two measurements complement each other by probing different spectral regions, and consequently, VCD signal intensities should not be compared between the two observed spectra. KBr pellets can easily show birefringence artifacts, which is probably the case in the 1000−1100 cm^{-1} region, and possibly other spectral regions as well. The noise level does not identify such artifacts.

Synthesis of Hinokiresinol. (*E*)-1,3-Bis(4-[(tetrahydro-2*H*-pyran-2-yl)methyl]phenyl)pent-4-en-1-one (6). A solution of vinylmagnesium bromide (1.0 M solution in THF, 60.0 mmol, 60.0 mL), in an inert nitrogen atmosphere, was added to a suspension of cuprous iodide (2.7 mmol, 0.520 g) in THF (60 mL) and cooled to 0 °C. After stirring for 15 min at 0 °C a solution of (*E*)-1,3-bis(4-[tetrahydro-2*H*-pyran-2-yloxy]phenyl)-prop-2-en-1-one (**5**)[24] (11.13 g, 27.3 mmol) in THF (30 mL) was added to the reaction mixture, and the mixture was stirred for an additional 2 h at 0 °C. After quenching with an aqueous saturated NH_4Cl solution the mixture was diluted with Et_2O (400 mL) and successively washed twice with water (400 mL)

Scheme 1

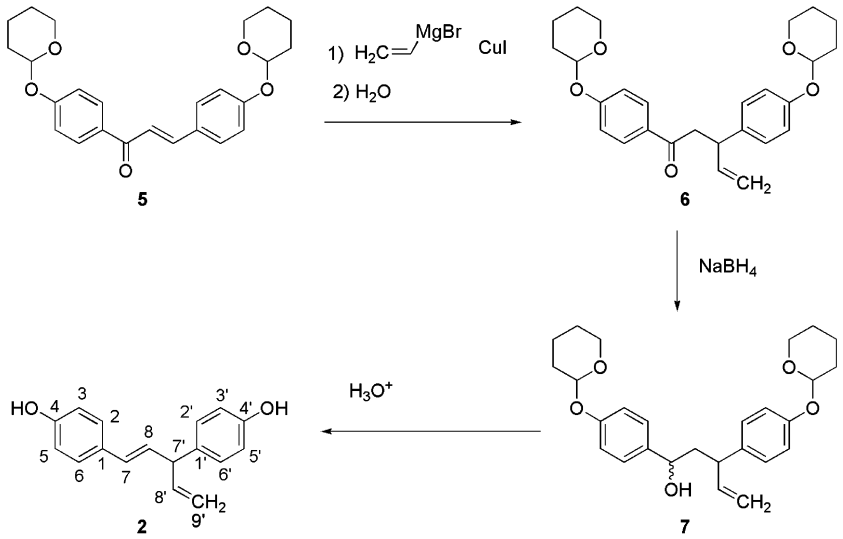

and once with brine (200 mL). The organic layer was dried over Na_2SO_4, filtered, and concentrated in vacuo. The product was purified by column chromatography using toluene−EtOAc (20:1) as an eluent to give **6** (7.47 g, 75%) as pale yellow crystals, mp 92−94 °C (MeOH): ^{1}H NMR ($CDCl_3$, 300 MHz) δ 1.55−2.05 (12H, m, CH_2 groups from THP); 3.26 (1H, dd, J = 6.6, 16.8 Hz, H-8); 3.35 (1H, dd, J = 7.8, 16.8 Hz, H-8); 3.56−3.64 (2H, m, OCH_2 groups from THP); 3.81−3.94 (2H, m, OCH_2 groups from THP); 4.07 (1H, ddd, J = 7.2 Hz, H-7′); 4.99 (1H, d, J = 17.4 Hz, H-9′); 5.03 (1H, d, J = 10.2 Hz, H-9′); 5.37 (1H, ddd, J = 3.0 Hz, O_2CH group from THP); 5.51 (1H, ddd, J = 3.0 Hz, O_2CH group from THP); 6.01 (1H, ddd, J = 6.6, 10.8, 17.4 Hz, H-8′); 6.98 (2H, d, J = 8.7 Hz, H-3′, H-5′); 7.06 (2H, d, J = 8.7 Hz, H-3, H-5); 7.16 (2H, d, J = 8.4 Hz, H-2′, H-6′); 7.90 (2H, d, J = 8.4 Hz, H-2, H-6).

***(E)*-1,3-Bis(4-[(tetrahydro-2*H*-pyran-2-yl)methyl]phenyl)pent-4-en-1-ol (7).** $NaBH_4$ (3.24 g, 85.6 mmol) was added to a solution of **6** (7.47 g, 17.1 mmol) in EtOH (150 mL), and the solution was stirred overnight at room temperature. The reaction mixture was quenched with an aqueous solution of NaOH (5%, 300 mL), and the mixture was extracted twice with Et_2O (150 mL). The combined organic layers were dried over Na_2SO_4, filtered, and concentrated in vacuo. The product was purified by column chromatography using toluene−EtOAc (9:1) as an eluent to give a mixture of the diastereomers as a yellow syrup (7.20 g, 96%): ^{1}H NMR ($CDCl_3$, 300 MHz) δ 1.56−2.34 (14H, m, H-8 + CH_2 groups from THP); 3.32 (ddd, J = 7.5 Hz); 3.44 (ddd, J = 8.1 Hz) (1H all together, H$^{7'}$); 3.56−3.60 (2H, m, OCH_2 groups from THP); 3.84−3.93 (2H, m, OCH_2 groups from THP); 4.43 (dd, J = 6.0 Hz); 4.54 (dd, J = 6.0 Hz) (1H all together, H-7); 4.96−5.06 (2H, m, H-9′); 5.36−5.40 (2H, m, O_2CH groups from THP); 5.89 (ddd, J = 7.5, 9.9, 17.4 Hz); 5.96 (ddd, J = 7.5, 9.9, 17.4 Hz) (1H all together, H-8′); 6.95−7.23 (8H, m, H-2, H-3, H-5, H-6, H-2′, H-3′, H-5′, H-6′).

Hinokiresinol (2) (racemic). To a solution of the alcohol **7** (7.19 g, 16.4 mmol) in MeOH (150 mL) was added a 7% aqueous solution of HCl (85 mL), and the mixture was refluxed for 1 h. After cooling it was poured into a saturated aqueous $NaHCO_3$ solution (500 mL). The mixture was extracted twice with CH_2Cl_2 (200 mL). The combined organic layers were washed with brine (200 mL), dried over Na_2SO_4, filtered, and concentrated in vacuo. The product was purified by column chromatography using toluene−EtOAc (9:1) to give racemic **2** as colorless crystals, which over time turned red (1.93 g, 47%), mp 69−71 °C ($CHCl_3$): ^{1}H NMR (acetone-d_6, 300 MHz) δ 4.12 (1H, t, J = 6.9 Hz, H-7′); 5.09 (2H, m, H-9′); 6.09 (1H, ddd, J = 6.9, 9.9, 17.7 Hz, H-8′); 6.26 (1H, dd, J = 6.9, 15.9 Hz, H-8); 6.36 (1H, d, J = 16.2 Hz, H-7); 6.78 (2H, d, J = 8.7 Hz, H-3′, H-5′); 6.80 (2H, d, J = 9.0 Hz, H-3, H-5); 7.10 (2H, d, J = 8.7 Hz, H-2′, H-6′); 7.27 (2H, d, J = 9.0 Hz, H-2, H-6); 8.24 (1H, s, br, OH); 8.41 (1H, s, br, OH)

Optical Resolution of Hinokiresinol (2). Racemic hinokiresinol was resolved over a Daicel Chiralcel OD 0.46 × 25 cm chiral column using petroleum ether−2-propanol (94:6) with added HOAc (0.4%) as an eluent and a flow of 1 mL/min. The two enantiomers eluted with retention times of 64.2 min ($[\alpha]_D^{25}$ −1.7° (*c* 0.27, acetone)), lit.[25] −3°) and 71 min ($[\alpha]_D^{25}$ +4.4° (*c* 0.38, acetone)).

Antiplasmodial Assay. The antiplasmodial activity toward the chloroquine-sensitive 3D7 *Plasmodium falciparum* strain (IC_{50} 24 nM) was determined as previously described.[26] The experiments were performed three times, each time in triplicate.

Acknowledgment. This work was supported by the Danish Ministry of Science Technology and Innovation and by the Lundbeck Foundation. P.-O. Norrby from the Technical University of Denmark is acknowledged for assistance with MacroModel. P. W. Thulstrup, The Royal Veterinary and Agricultural University, is acknowledged for help with the electronic CD measurements. The Jmol development team (http://jmol.sourceforge.net) is acknowledged for their molecular visualization software.

References and Notes

(1) Minami, E.; Taki, M.; Takaishi, S.; Iijima, Y.; Tsutsumi, S.; Akiyama, T. *Chem. Pharm. Bull.* **2000**, *48*, 389−392.
(2) Oketch-Rabah, H. A.; Dossaji, S. F.; Christensen, S. B.; Frydenvang, K.; Lemmich, E.; Cornett, C.; Olsen, C. E.; Chen, M.; Kharazmi, A.; Theander, T. *J. Nat. Prod.* **1997**, *60*, 1017−1022.
(3) Ameer, F.; Drewes, S. E.; Drewes, M. W.; Roos, G. H. P.; Watson, M. C. *J. Chem. Soc., Perkin Trans. 1* **1988**, 1425−1430.
(4) Beracierta, A.; Whiting, D. *J. Chem. Soc., Perkin Trans. 1* **1978**, 1257−1263.
(5) Beracierta, A.; Whiting, D. A. *Tetrahedron Lett.* **1976**, 2367−2370.
(6) Hirose, Y.; Oishi, N.; Nagaki, H.; Nakatsuka, T. *Tetrahedron Lett.* **1965**, 3665−3668.
(7) Erdtman, H.; Harmatha, J. *Phytochemistry* **1979**, *18*, 1495−1500.
(8) Enzell, C. R.; Hirose, Y.; Thomas, B. R. *Tetrahedron Lett.* **1967**, 793−798.
(9) Tsui, W.; Brown, G. D. *Phytochemistry* **1996**, *43*, 1413−1415.
(10) Jeong, S.-J.; Higuchi, R.; Ono, M.; Kuwano, M.; Kim, Y. C.; Miyamoto, T. *Biol. Pharm. Bull.* **2003**, *26*, 1721−1724.
(11) Iida, Y.; Oh, K.-B.; Saito, M.; Matsuoka, H.; Kurata, H.; Natsume, M.; Abe, H. *J. Agric. Food Chem.* **1999**, *47*, 584−587.
(12) Hirose, T.; Oishi, N.; Nagaki, H.; Nakatsuka, T. *Tetrahedron Lett.* **1965**, 3665−3668.
(13) Freedman, T. B.; Cao, X. L.; Dukor, R. K.; Nafie, L. A. *Chirality* **2003**, *15*, 743−758.
(14) Hirose, Y.; Ishikawa, K.; Nakatsuka, T. *Agric. Biol. Chem.* **1968**, *32*, 1283−1286.
(15) Hishiyama, S.; Kato, A.; Lee, S. S. *Tennen Yuki Kagobutsu Toronkai Koen Yoshishu* **1998**, *40*, 625−630.
(16) Nafie, L. A.; Buijs, H.; Rilling, A.; Cao, X. L.; Dukor, R. K. *Appl. Spectrosc.* **2004**, *58*, 647−654.
(17) Nafie, L. A. *Appl. Spectrosc.* **2000**, *54*, 1634−1645.

(18) Mohamadi, F.; Richards, N. G. J.; Guida, W. C.; Liskamp, R.; Lipton, M.; Caufield, C.; Chang, G.; Hendrickson, T.; Still, W. C. *J. Comput. Chem.* **1990**, *11*, 440−467.
(19) Frisch, M. J.; Trucks, G. W.; Schlegel, H. B.; Scuseria, G. E.; Robb, M. A.; Cheeseman, J. R.; Montgomery, J. A., Jr.; Vreven, T.; Kudin, K. N.; Burant, J. C.; Millam, J. M.; Iyengar, S. S.; Tomasi, J.; Barone, V.; Mennucci, B.; Cossi, M.; Scalmani, G.; Rega, N.; Petersson, G. A.; Nakatsuji, H.; Hada, M.; Ehara, M.; Toyota, K.; Fukuda, R.; Hasegawa, J.; Ishida, M.; Nakajima, T.; Honda, Y.; Kitao, O.; Nakai, H.; Klene, M.; Li, X.; Knox, J. E.; Hratchian, H. P.; Cross, J. B.; Adamo, C.; Jaramillo, J.; Gomperts, R.; Stratmann, R. E.; Yazyev, O.; Austin, A. J.; Cammi, R.; Pomelli, C.; Ochterski, J. W.; Ayala, P. Y.; Morokuma, K.; Voth, G. A.; Salvador, P.; Dannenberg, J. J.; Zakrzewski, V. G.; Dapprich, S.; Daniels, A. D.; Strain, M. C.; Farkas, O.; Malick, D. K.; Rabuck, A. D.; Raghavachari, K.; Foresman, J. B.; Ortiz, J. V.; Cui, Q.; Baboul, A. G.; Clifford, S.; Cioslowski, J.; Stefanov, B. B.; Liu, G.; Liashenko, A.; Piskorz, P.; Komaromi, I.; Martin, R. L.; Fox, D. J.; Keith, T.; Al-Laham, M. A.; Peng, C. Y.; Nanayakkara, A.; Challacombe, M.; Gill, P. M. W.; Johnson, B.; Chen, W.; Wong, M. W.; Gonzalez, C.; Pople, J. A. *Gaussian 03, Revision B.04*; Gaussian, Inc.: Wallingford, CT, 2004.
(20) Becke, A. D. *J. Chem. Phys.* **1993**, *98*, 5648−5652.
(21) Hariharan, P.; Pople, J. A. *Theor. Chim. Acta* **1973**, *28*, 213−222.
(22) Kendall, R. A.; Dunning, T. H.; Harrison, R. J. *J. Chem. Phys.* **1992**, *96*, 6796−6806.
(23) Cossi, M.; Scalmani, G.; Rega, N.; Barone, V. *J. Chem. Phys.* **2002**, *117*, 43−54.
(24) Severi, F.; Costantino, L.; Benvenuti, S.; Vampa, G.; Mucci, A. *Med. Chem. Res.* **1996**, *6*, 128−136.
(25) Minami, E.; Taki, M.; Takaishi, S.; Ijima, Y.; Tsutsumi, S.; Akiyama, T. *Chem. Pharm. Bull.* **2000**, *48*, 389−392.
(26) Ziegler, H.; Stærk, D.; Christensen, J.; Hviid, L.; Hägerstrand, H.; Jaroszewski, J. W. *Antimicrob. Agents Chemother.* **2002**, *46*, 1441−1446.

NP0502995